ARTICLE

Large-Area, Near-Infrared (IR) Photonic Crystals with Colloidal Gold Nanoparticles Embedding

Shobha Shukla,[†,‡] Alexander Baev,[‡] Hongsub Jee,[†] Rui Hu,[‡] Ryszard Burzynski,[§] Yong-Kyu Yoon,[†] and Paras N. Prasad*[,†,‡,§,∥]

Department of Electrical Engineering, Institute for Lasers, Photonics and Biophotonics, and Department of Chemistry, University at Buffalo, State University of New York, Buffalo, New York 14260, and Laser Photonics Technology, Inc., 1576 Sweet Home Road, Amherst, New York, 14228

ABSTRACT A polymeric composite material composed of colloidal gold nanoparticles (<10 nm) and SU8 has been utilized for the fabrication of large-area, high-definition photonic crystal. We have successfully fabricated near-infrared photonic crystal slabs from composite materials using a combination of multiple beam interference lithography and reactive ion etching processes. Doping of colloidal gold nanoparticles into the SU8 photopolymer results in a better definition of structural features and hence in the enhancement of the optical properties of the fabricated photonic crystals. A 2D air hole array of triangular symmetry with a hole-to-hole pitch of ~500 nm has been successfully fabricated in a large circular area of 1 cm diameter. Resonant features observed in reflectance spectra of our slabs are found to depend on the exposure time, and can be tuned over a range of near-infrared frequencies.

KEYWORDS: photonic composite materials • gold nanoparticles • lithography • photonic crystal • structural/optical properties

INTRODUCTION

Photonic composite materials, such as polymers doped with nanoparticles, have recently attracted a great deal of attention because of the relative ease and flexibility of their engineering as well as improved performance for application in photonic or optoelectronic devices, biosensors, etc. (1−10). Several properties of polymers such as porosity and mechanical, optical, or electrical properties can be easily modified by incorporating metal or dielectric nanoparticles (4−12). SU8 photo polymer is well-recognized in MEMS industry, because of its good chemical/biochemical and mechanical stability and its high optical transparency in the ultraviolet (UV) and visible-light regions. A major drawback of SU8 is its shrinkage after post-baking (95 °C), which results in high stress; this behavior affects more nanoscale-ordered patterned structures (9, 10). Dispersion of noble metal nanoparticles into the polymer alters its orientation and morphology, and quite often introduce great differences in physical properties of their constituents (7, 9−11). It has been reported earlier that the incorporation of gold nanopowder (>100 nm) into a polymeric matrix allows for better defined patterns with reduced stress (10). However, to limit the scattering due to incorporation of nanoparticles, the size of the nanoparticles should be less than 100 nm. Because of the small size of the nanoparticles (few tens of nanometer), they are uniformly dispersed in the microdomain of the polymer, thus establishing a means of harnessing both enthalpic and entropic interactions, and thereby influencing the macroscopic behavior of the composite material (11, 12). Hence doping of ultrasmall nanoparticles into the polymer is required for making high-quality photonic crystals (PhCs) and nanophotonic devices (9−13).

PhCs are periodic dielectric structures spanning in one, two, or three dimensions (1). They exploit the contrast of the refractive indices of their constituent domains to control the propagation of light, thus offering the distinct capability of modifying the density of electromagnetic modes (2−6). Losses are inevitably high in periodic structures with high refractive index contrast. However, by altering the geometry, a desirable band gap can be acquired even in materials with a low refractive index contrast. For example, one can achieve omni-directional photonic band gap in an SU8 epoxy resin (refractive index ~1.7) photonic structure with triangular air hole symmetry (5, 7, 8). PhCs, utilizing the richness and flexibility of organic optical materials offers unique opportunities toward the development of high-performance photonic devices (2−5).

The periodic structures can be achieved in a composite material using either electron beam lithography or two-photon absorption lithography or multiple interference beam lithography (MIL). MIL is generally considered an efficient, cost-effective, and therefore commercially manufacturable way to produce two-dimensional (2D) PhCs over a large area. This method provides a precise control of geometry and volume fraction, which is highly desirable for practical/

* Corresponding author. E-mail: pnprasad@buffalo.edu. Web: www.photonics.buffalo.edu. Phone: (716) 645-6800, ext. 2099. Fax: (716) 645-6945.

Received for review February 6, 2010 and accepted March 3, 2010

† Department of Electrical Engineering, University at Buffalo.

‡ Institute for Lasers, Photonics and Biophotonics, University at Buffalo.

§ Laser Photonics Technology.

∥ Department of Chemistry, University at Buffalo.

DOI: 10.1021/am100109f

Published on Web 03/11/2010

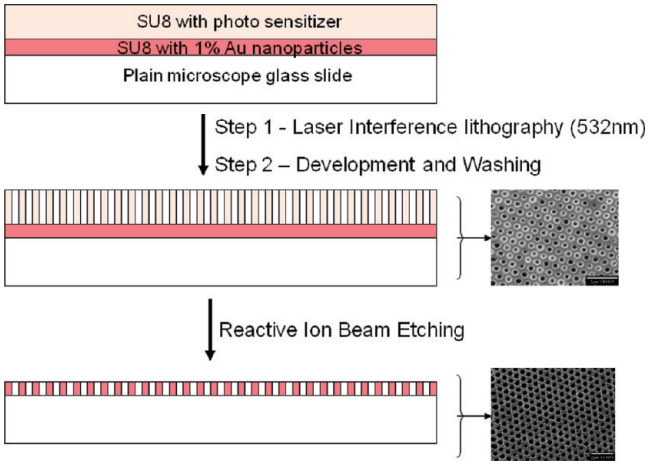

FIGURE 1. Schematics of photonic crystal fabrication using MIL and RIE processes.

commercial applications (8, 13). Typically, 2D array polymer structures, fabricated using MIL, do not have smooth sidewalls when the constituent polymer thickness is on the order of the wavelength of the incident light. To improve the shape, a pattern transfer technique using reactive ion beam etching (RIE) has been developed by our group recently to transfer the pattern from top layer to the bottom layer (7).

In this article, we have studied the structural/optical properties of colloidal gold nanoparticles (<10 nm) doped SU8 PhCs by fabricating large area (1 cm diameter circle) 2D slab using MIL and subsequent RIE. Dark-field microscopy images were taken to show an uniform dispersion of colloidal gold nanoparticles in the polymeric matrix. We have also investigated the influence of gold nanoparticles incorporation in SU8 on the optical properties of fabricated PhCs. Reflectance and absorbance spectra were examined to characterize the structures. Scanning electron microscopy imaging was utilized to quantify the periodicity and uniformity of the pattern.

RESULTS AND DISCUSSION

Figure 1 shows the procedure for photopatterning and transferring the pattern to the gold-doped polymer layer. A double layer fabrication scheme was utilized for transferring the pattern to bottom layer, i.e., gold nanoparticles doped polymer layer (from here on called the composite layer) (7, 14). The composite layer was overcoated with a photosensitive layer. Photosensitive layer was patterned via multiple laser beam interference to create a large-area mask. Pattern was transferred from the top layer to the bottom layer via RIE. After being cured and cooled down, the patterned samples were stored in dehydrated chambers for further characterization. There was no evidence of sample degradation even after storage for a longer period of time (~6 months). Figure 2 shows the dark-field image of the gold-nanoparticle-doped polymer film that is used as a bottom layer of the proposed structure. It is clear that the nanoparticles are uniformly dispersed in the polymer.

Figure 3a shows the TEM and HRTEM images of the prepared gold nanoparticles (Au NPs) with the average

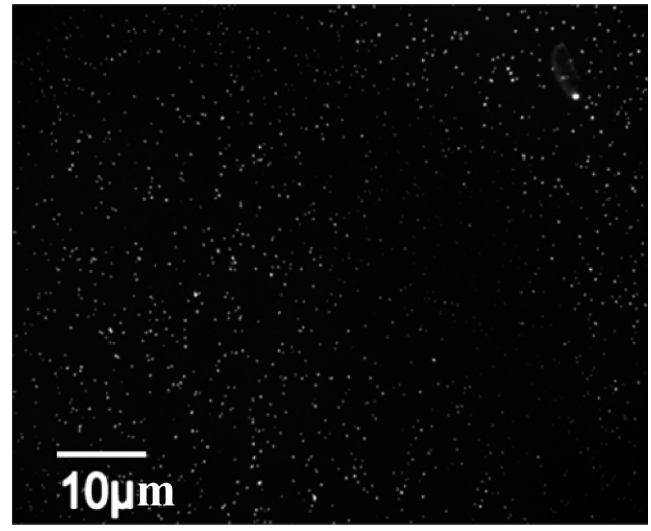

FIGURE 2. Dark-field image of unpatterned SU8 film doped with 1 wt % gold nanoparticles.

diameter between 7 and 8 nm, Figure 3b presents the absorption spectra of the colloidal gold nanoparticles with the characteristic surface plasmon resonance (SPR) peak centered at around 530 nm, and Figure 3c demonstrates the diffraction pattern from the fabricated PhC illuminated with the 457 nm laser beam, with a beam size large enough to illuminate whole area of PhC. The diffraction pattern was obtained from a sample with the area of 0.2 cm^2, as after final fabrication the whole sample was divided in 4 parts for further optical characterization.

The diffraction pattern consists of 6 bright spots, though one spot is not visible in Figure 3c, as it was shadowed by the stand holding the PhC. The diffraction pattern from the triangular lattice PhC with the regular spacing of bright spots clearly indicates that the pattern is very uniform and has the hexagonal symmetry with domains having the same crystallographic orientation that is very typical of single crystals (15).

Figure 4 shows the scanning electron microscopy (SEM) images of (a) the SU8 PhC and (b) the gold-nanoparticle-doped SU8 PhC, with a hole-to-hole pitch of ~500 nm. It is quite evident from the SEM images that the presence of gold nanoparticles helps in defining the pattern. This is further confirmed by examining the distribution of eccentricities of holes contained within two equal spots of the crystals (histograms in Figure 5). As one can see, the number of holes with small eccentricities is greater for the gold-nanoparticle-doped PhC. Required laser exposure time for photopolymerizing the top layer was reduced from ~8 s in undoped polymer layer to ~5 s in gold doped polymer layer. We attribute enhanced geometry to the high specific heat capacity (0.128 J/g °C) of the gold nanoparticles, because of which they function as a heat sink for the unwanted heat gradients while performing RIE; this ultimately results in enhanced circular symmetry of the air holes in gold-nanoparticle-doped SU8 PhC. Enhanced absorption of laser light by the gold nanoparticles present in the polymeric matrix should also help in improving the crystal geometry, as the plasmonic peak of the gold nanoparticles (530 nm) coincides

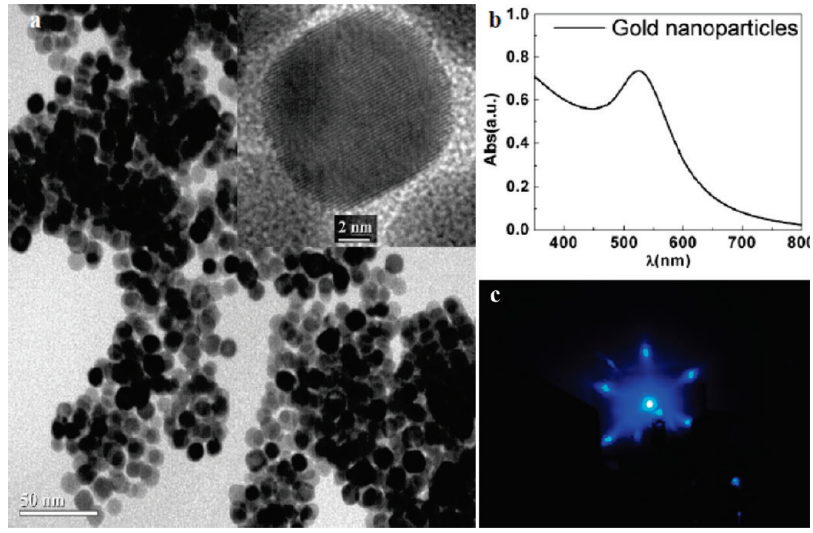

FIGURE 3. (a) TEM image of gold nanoparticles (inset, HRTEM), (b) absorption spectrum of gold nanoparticles, (c) diffraction pattern from photonic crystal.

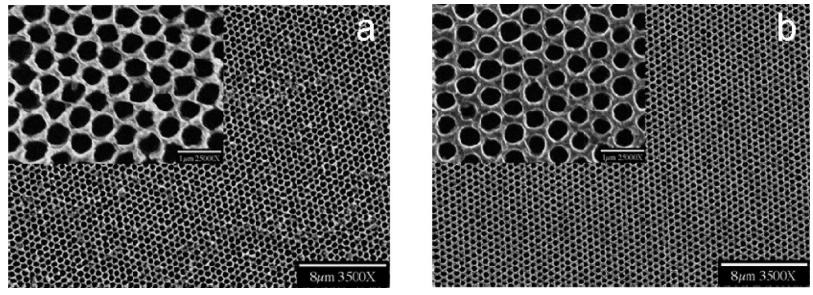

FIGURE 4. SEM image of (a) SU8 PhC, (b) gold-nanoparticle-doped SU8 PhC.

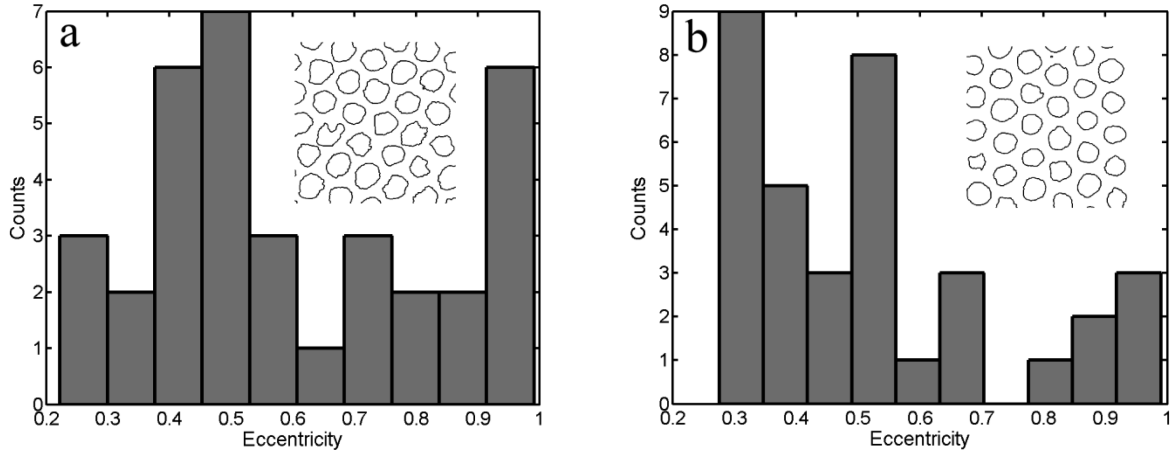

FIGURE 5. (a) Eccentricity of the holes histogram for SU8 PhC; (b) eccentricity of the holes histogram for gold-nanoparticle-doped SU8 PhC; insets show processed SEM images.

with the laser wavelength that we used for photolithography (532 nm). However, attempts to record the plasmonic peak with the spectrometer were not successful. We tentatively attribute this to instrument limitation as the nanoparticles loading were small (1 % by weight).

Optical properties of the sample were studied by measuring spectral reflectance using a UV−vis spectrophotometer in the wavelength range from near-infrared to ultraviolet. The incidence angle was set to 2.5° with the respect to the normal to the patterned surface. In the PhCs, wave vector takes the form $K_i + G$, where K_i is the initial wavevector and G is reciprocal lattice vector. For the incidence angle of 2.5°, parallel component of K_i is very small but G still provides some nonzero values (16). Illuminated area for all the spectroscopic characterization was about 0.2 cm^2. For reference, we have recorded the reflectance spectra of all reference layers (see the Supporting Information). Reference/background correction was done using a plain glass substrate in all the cases. In the UV−vis spectrophotometer, grating and photodetector change took place at the wavelength of 700 nm, as evidenced by the observation of a noise near that wavelength in all the spectra. By varying the grating and

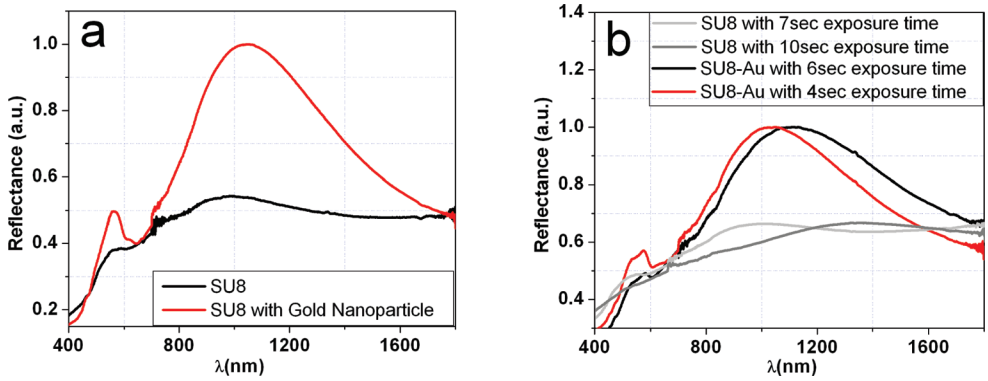

FIGURE 6. (a) Reflectance spectra of SU8 PhC and gold-nanoparticle-doped SU8 PhC; (b) effect of exposure time on reflectance of SU8 PhC and gold-nanoparticle-doped SU8 PhC.

detector change position to various wavelengths values near 700 nm, we confirmed that there is no reflectance feature near 700 nm from the PhC itself. The reflectance features were greatly enhanced in the gold nanoparticles doped PhC (Figure 6a). The 2-fold enhancement factor can be attributed to a better definition of the PhC structures produced by the presence of gold nanoparticles. Even with the greatly improved structures in samples doped with the gold nanoparticles, nonuniformity over a large area (remember that the reflectance spectra is collected from the whole 0.2 cm^2 area) could not be completely alleviated, thus resulting in spectral broadening. The first resonant feature is centered at 1050 nm, whereas the second one is around 570 nm.

The effect of laser exposure time on PhCs was also studied. With a small variation in the exposure time above a certain threshold value, corresponding to the radiation dose above which the polymerization begins, one can tune the PhC stop bands to the desired wavelength position. As shown in Figure 6b, by increasing the exposure time by 2−3 s above the threshold value (corresponding to the beginning of photopolymerization), the peak wavelength of the stop band can be red-shifted. The reason for the red shift is smaller holes size due to the increased energy uptake by SU8 polymer from ~1 J/cm^2 to ~1.5 J/cm^2 (negative photoresist). The band structure calculations confirmed that increase of the radius-to-pitch ratio results in a blue shift of the stop bands. PhC obtained with even longer exposure time deliver more red-shifted but comparatively inferior optical quality spectra than the optimum exposure time PhC, tentatively attributed to unwanted heat propagation in PhC that destroys the pattern.

Finally, Figure 7 shows the TE/TM band structure diagram of an ideal hexagonal PhC, which was calculated using commercial software package RSoft (17). The ratio of the hole radius to the lattice constant was set to 0.4, and dielectric constant of 3.2 was assigned to SU8. The actual radius to lattice constant ratio is also in good agreement with this value as estimated from the SEM images. Two stop bands are identified, the TE stop band in the frequency range of 0.45 to 0.5, and a narrow TM stop band in the frequency range of 1.125 to 1.15. The positions of the stop bands coincide with the experimental reflection peaks at ~1050 and 570 nm. The abundance of leaky modes close to the

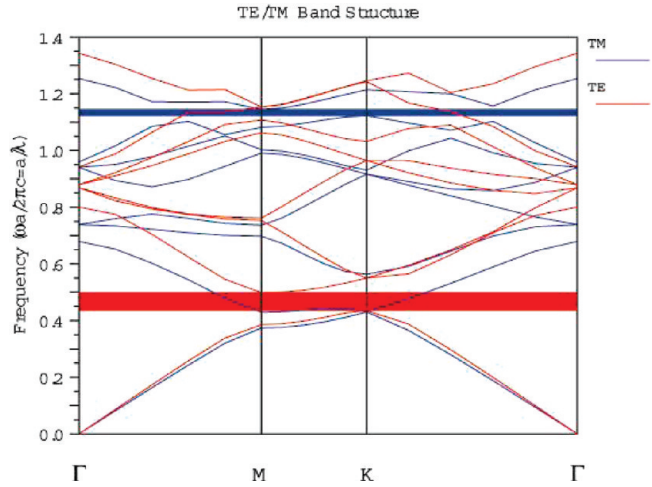

FIGURE 7. Computed band structure of SU8 PhC.

Γ-point around the second-order stop band explains relatively narrow resonant feature at around 570 nm. At the same time, the leaky modes of the slab around the first stop band are spaced farther apart, giving rise to a broad resonant feature centered at around 1050 nm. Gold doping was not considered in the calculations. Our estimation based on the effective medium theory showed that a small change in the effective dielectric permittivity of SU8 (with the addition of low volume fraction of gold nanoparticles) will not result in substantial change in the position of the stop bands. This observation is consistent with our experimental results.

CONCLUSION

In this article, we have demonstrated that colloidal gold nanoparticle (<10 nm) doped SU8 composite material PhC have better structural and optical properties as compared to undoped SU8 PhC. Gold nanoparticles enhance the absorption of photo patterning laser light as well as reduce the unwanted heat propagation, while performing RIE, and thus improve the overall quality of the PhC. We have successfully fabricated large-area, high-definition tunable near-infrared PhCs with triangular lattice of air hole design, based on colloidal gold-nanoparticle-doped (<10 nm) SU8 polymer. Detailed studies have been performed to investigate various parameters affecting the crystal geometry and optical properties. The scanning electron microscopy images are in good

agreement with the results obtained from optical characterization and numerical simulations. Our method paves the pathway to the time- and cost-effective fabrication of good-quality and large-area-tunable PhCs.

EXPERIMENTAL SECTION

The polymer SU8 was purchased from MicroChem Inc. and the gold nanoparticles in the organic phase were prepared by the previously reported method (12). To fabricate the composite periodic structure, we loaded the gold nanoparticles into the polymeric matrix. Gold nanoparticles were suspended in chlorobenzene, which is compatible with cyclopentanone, the solvent for SU8. A 10 wt % SU8 solution with a small amount of photosensitizer was prepared and mixed via ultrasonication with gold nanoparticles (1 wt % SU8), slowly and dropwise, and immediately spin-coated at 3500 rpm onto a precleaned glass substrate. This bottom composite layer was then polymerized, cured, and cooled to the room temperature. The thickness of this layer was around 200 nm.

The exact recipe for preparing a photosensitive layer is described elsewhere (7) and we give only a brief description here. SU8 was mixed with a photosensitizer (Rubrene (Sigma-Aldrich)) and a photoacid generator (diaryliodonium hexafluoroantimonate (Polyset PC-2506)). Tributylamine, which functions as a photoinhibitor, was also admixed. The 35 wt % SU8 solution was spin-coated on the composite bottom layer at 2500 rpm to achieve a thickness of approximately 800 nm. After curing, it is normally difficult to remove SU8, thus no washing off was observed for the second layer coating. After spin-coating the top photosensitive layer, the film was baked on a hot plate at 65 and 95 °C successively to remove any excess amount of the solvent from the film. After being cooled to room temperature, the film was exposed to the laser light (532 nm). The exposure dose used was between 1 and 2J/cm^{-2}. Three beams laser interference lithography was employed to pattern the film.

A continuous wave Nd:YVO4 laser (Coherent Verdi V6), operating at 532 nm, was used for creating the interference pattern. Laser beams formed 120° angles between each other, and the incident angle between the beams and the normal to the substrate was 23°. All three beams interfered within the sample plane to create a spatial variation of intensity. After exposure, the film was postbaked on a hot plate at 75.5 °C for a short period of time, allowed to cool for 5−10 min, and then dipped in propylene glycol monoether acetate (PGMEA) to remove the unpolymerized part of SU8. Final washing was carried out in isopropanol.

Finally, RIE was used to transfer the pattern to the bottom layer using the top layer as a mask. A radio frequency (RF) power of 80 W was used for etching with the etching time of 1 min. The RIE was performed with a benchtop RIE system (RIE-1C; SAMCO Inc.). The oxygen flow rate was 12.5 sccm and the CF_4 flow rate was tuned to 3.0 sccm. It is worthwhile to note that one can simultaneously realize the pattern transfer and mask removal by properly designing film properties and process parameters, as reported in our previous publication (7).

Acknowledgment. The authors are grateful to Dr. E. Furlani for valuable discussions. This work was supported by a grant (FA95500910258) from the Chemistry and Life Sciences Directorate of the Air Force office of Scientific Research and in part by National Science Foundation CAREER program (ECCS 0748153).

Supporting Information Available: Reflectance spectra of the reference layers; Reflectance spectra of SU8-Au PhC obtained with unpolarized, s-polarized (TM), and p-polarized (TE) light (PDF). This material is available free of charge via the Internet at http://pubs.acs.org.

REFERENCES AND NOTES

(1) Prasad, P. N. *Nanophotonics*; Wiley-Interscience: Hoboken, NJ, 2004.
(2) Lodahl, P.; Floris, van Driel, A.; Nikolaev, I. S.; Irman, A.; Overgaag, K.; Vanmaekelbergh, D.; Vos, W. L. *Nature* **2004**, *430*, 654–57.
(3) Martiradonna, L.; Carbone, L.; Tandaechanurat, A.; Kitamura, M.; Iwamoto, S.; Manna, L.; De, Vittorio, M.; Cingolani, R.; Arakawa, Y. *Nano Lett.* **2008**, *8*, 260–64.
(4) Kress, A.; Hofbauer, F.; Reinelt, N.; Kaniber, M.; Krenner, H. J.; Meyer, R.; Böhm, G.; Finley, J. J.*Phys. Rev. B* **2005**, *71*, 241304–8.
(5) Guven, K.; Ozbay, E. *J. Opt. A: Pure Appl. Opt.* **2007**, *9*, 239–47. Braun, P. V.; Zehner, R. W.; White, C. A.; Weldon, M. K.; Kloc, C.; Patel, S. S.; Wiltzius, P. *Europhys. Lett.* **2001**, *56*, 207–213.
(6) Yablonovitch, E. *J. Phys.: Condens. Mater.* **1993**, *16*, 2443–60. Miyake, M.; Chen, Y. C.; Braun, P. V.; Wiltzius, P. *Adv. Mater.* **2009**, *21*, 3012.
(7) Zhang, A. P.; Burzynski, R.; Yoon, Y. K.; Prasad, P. N.; He, S. *Opt. Lett.* **2008**, *33*, 1303–1305.
(8) Escuti, M. J.; Crawford, G. P. *Opt. Eng.* **2004**, *43*, 1973–87.
(9) Jiguet, S.; Bertsch, A.; Judelewicz, M.; Hofmann, H.; Renaud, P. *Microelectron. Eng.* **2006**, *83*, 1966–70.
(10) Chiamori, H. C.; Adhiprakasha, E. V.; Hantsoo, E. T.; Straalsund, J. B.; Melosh, N. A.; Pruitt, B. L. *Microelectron. J.* **2007**, *39*, 228.
(11) Balazs, A. C.; Emrick, T.; Russell, T. P. *Science* **2006**, *314*, 1107.
(12) Gupta, S.; Zhang, Q.; Emrick, T.; Balazs, A. C.; Russell, T. P. *Nat. Mater.* **2006**, *5*, 229.
(13) Haske, W.; Chen, V. W.; Hales, J. M.; Dong, W.; Barlow, S.; Marder, S. R.; Perry, J. W. *Opt. Exp.* **2007**, *15*, 3426–36.
(14) Yong, K. T.; Sahoo, Y.; Swihart, M. T.; Prasad, P. N. *Adv. Mater.* **2006**, *18*, 1978–82.
(15) Sinitskii, A.; Abramova, V.; Laptinskaya, T.; Tretyakov, Y. D. *Phys. Lett. A* **2007**, *366*, 516–522.
(16) García-Santamaría, F.; Galisteo-López, J. F.; Braun, P. V.; López, C. *Phys. Rev. B* **2005**, *71*, 195112–195117.
(17) www.rsoft.com.

AM100109F